Icarus

Visible and Near-InfraRed (VNIR) reflectance of silicate glasses: characterization of a featureless spectrum and its implications for planetary geology.

--Manuscript Draft--

Manuscript Number:	ICARUS-D-21-00299
Article Type:	Research paper
Keywords:	Experimental techniques; Terrestrial planets; Volcanism
Corresponding Author:	alessandro pisello ITALY
First Author:	Alessandro Pisello, Dr.
Order of Authors:	Alessandro Pisello, Dr.
	Simone De Angelis
	Marco Ferrari
	Massimiliano Porreca
	Francesco Pasqualino Vetere
	Maria Cristina De Sanctis
	Diego Perugini
Abstract:	Silicate glasses represent a major component in volcanic products, both in pyroclastic deposits and lavas. To date, their spectral characteristics are not thoroughly investigated in the context of their characterization as possible analogues of planetary surfaces, mainly due to their lack of spectral features. Nevertheless, featureless VIS-NIR spectra for which it is only possible to retrieve relative parameters (slope, albedo) are commonly observed on the surface of planetary bodies, and volcanic structures are supposed to be widely present in all terrestrial planets within the Solar System. Therefore, the correct interpretation of their geochemical signature is important in the attempt to shed new light on the evolution of these planets, and detailed knowledge about of spectral response of silicate glasses is fundamental for such a purpose.
Suggested Reviewers:	Rachel Klima Rachel.Klima@jhuapl.edu
	Katrin Stephan katrin.stephan@dlr.de
	Faith Vilas fvilas@psi.edu
	Alessandro Vona alessandro.vona@uniroma3.it
	Sebastienne Besse sbesse@sciops.esa.int
Opposed Reviewers:	

Highlights for the submitted manuscript: "Visible and Near-InfraRed (VNIR) reflectance of silicate glasses: characterization of a featureless spectrum and its implications for planetary geology"

- Silicate glasses are an important constituent of igneous products, especially volcanic, yet they are not deeply investigated in terms of relationship between spectral response and chemical composition.
- Investigation of reflectance in the VNIR range is commonly performed on geologically relevant material to build up databases for the characterization of planetary surface.
- A series of 14 silicate glasses with complex chemical composition were produced starting from natural material with the aim to obtain large chemical variability by means of silica and alkaline content.
- Silicate glasses were characterized with reflectance in the VNIR, and parameterization allowed to individuate relationships between chemical composition and spectral characteristics (slope, albedo).
- Results from such investigation will be useful to interpret occurrence of volcaniclastic products on planetary surfaces.

Visible and Near-InfraRed (VNIR) reflectance of silicate glasses: characterization of a featureless spectrum and its implications for planetary geology

Pisello Alessandro[1], De Angelis Simone[2], Ferrari Marco[2], Porreca Massimiliano[1], Vetere Francesco Pasqualino[1-3], De Sanctis Maria Cristina[2], Perugini Diego[1].

1) Department of Physics and Geology, University of Perugia, I-06123 Perugia, Italy.
2) Institute for Space Astrophysics and Planetology (IAPS-INAF, Rome, Italy)
3) Institute of Mineralogy, Leibniz Universität Hannover, D-30167 Hannover, Germany.

Keywords: Experimental techniques, Terrestrial planets, Volcanism.

Abstract

Silicate glasses represent a major component in volcanic products, both in pyroclastic deposits and lavas. To date, their spectral characteristics are not thoroughly investigated in the context of their characterization as possible analogues of planetary surfaces, mainly due to their lack of spectral features. Nevertheless, featureless VIS-NIR spectra for which it is only possible to retrieve relative parameters (slope, albedo) are commonly observed on the surface of planetary bodies, and volcanic structures are supposed to be widely present in all terrestrial planets within the Solar System. Therefore, the correct interpretation of their geochemical signature is important in the attempt to shed new light on the evolution of these planets, and detailed knowledge about of spectral response of silicate glasses is fundamental for such a purpose.

In this study, experimental petrology techniques have been used to produce 15 silicate glasses having complex chemical composition corresponding to three of the most common magmatic series on planet Earth. These glasses have been investigated in the Visible and Near/Infrared range to observe and interpret the variation of slope, albedo, and spectral ratio $R_{1.55}/R_{0.8}$ as a function of chemical composition. We found that, despite the complexity of factors influencing the spectral response, a good correlation can be derived linking spectral parameters with both iron content and composite Silicium-Calcium-Iron-Magnesium content (SCFM parameter). Results presented in this work might represent the baseline for new research lines focused on deciphering the significance of silicate glasses in the context of planetary exploration, opening new windows to access information on planetary differentiation that cannot be obtained using only existing materials and methods.

1. Introduction

Spectroscopic investigations of geological materials for the characterization of possible analogues useful for planetary investigations within the Visible and Near-Infrared region (hereon, VNIR), have been extensively carried out mainly because electronic transitions of Fe or FeO occur within this range, allowing the identification of iron-bearing rocks (Adams 1967, Adams 1975). Indeed, the majority of planetary igneous rocks are supposed to have mafic or ultramafic bulk compositions, which means relatively low silica content (45-50 wt.%) and relatively high iron content (7-15 wt.%), making VNIR a particularly suitable spectral range for planetary geology research. Previous spectral investigations by VNIR spectroscopy regarded the main rock-forming minerals of mafic igneous rocks: olivine (Mustard et al. 2005, Mølholt et al. 2008, Isaacson et al. 2014, Penttilä et al. 2020), pyroxene (Pompilio et al. 2007, Klima et al. 2008, Klima et al. 2009, Markus et al. 2018) and An-rich plagioclase (Hiroi et al. 2012, Serventi et al. 2013, Carli et al. 2014,). Further, in order to provide insights on the possible traces of life on other planetary bodies, a great deal of work on other (also water-bearing) crystalline phases, formed through alteration of igneous minerals, has been performed. This is the case of various types of phyllosilicates like montmorillonite, chamosite, and nontronite (Poulet et al. 2005, Ferrari et al. 2019), serpentine-related hydrated silicates (Cloutis et al. 2018), and hydrated sulphate minerals like gypsum or kieserite (Gendrin et al. 2005, Murchie et al. 2009, De Angelis et al. 2017). Moreover, because of some putative carbonaceous-dominated areas on the planetary surfaces (Kargel et al. 1994, Wray et al. 2011, Boynton et al. 2009, Morris et al. 2010), even carbonaceous rocks were characterized in the VNIR region, taking into consideration carbonates hosting Fe, Mg, and Ca (Harner and Gilmore 2015, Bishop et al. 2011). Additional studies include VNIR investigations of rocks (i.e. mineral assemblages) such as meteorites (Gaffey 1976, Cloutis et al. 2011 and 2018), and igneous rocks, both intrusive and effusive, with composition ranging from mafic to felsic (Singer 1982, Evans et al. 1982, Crown and Pieters 1987, Walter and Salisbury 1989, Harloff and Arnold 2001, Anbazhagan and Arivazhagan 2010, Sgavetti et al. 2006).

Although existing literature offers a plethora of studies regarding crystalline phases (which can be associated with magmatism, volcanism, or alteration of such products), amorphous materials, such as glasses, are not widely taken into account. However, glasses represent an important volcanic product. Volcanic glasses can occur in a wide spectrum of effusive and rapidly cooled rocks, from pure glassy rocks (such as obsidian) to the large majority of volcanic rocks (often termed porphyric or hypocrystalline) that, therefore, can show variable volumes of interstitial glass or amorphous material.

Moreover, igneous products commonly show important variations of the spectral response not only with varying chemical composition but also as a function of the grain size of the investigated sample (De Angelis et al. 2014). This behaviour was also observed for glassy samples, where optical constants and particle size of glasses were retrieved from VNIR spectra (Carli et al. 2016). In addition, further studies on the VNIR reflectance of glasses were performed with various purposes:

Bell et al. (1976) and Wells and Hapke (1977) investigated lunar-like glasses to characterize changes in the spectral response with varying Fe or Ti contents and oxygen fugacity; Minitti et al. (2002) investigated the effects of crystallization on the spectral response; Moroz et al. (2009) focused on the influence of melting and cooling rates on the spectral response; Tompkins and Pieters (2010), studied possible lunar impact glasses; Cloutis et al. (1990) and Carli et al. (2014) observed substantial difference between the spectral response of crystalline and glass-bearing rocks; finally, Cannon et al. (2017) compared the spectral response of possible glasses with Lunar, Martian and Hermean compositions.

In this study, we aim at providing new and original data on VNIR spectroscopy of silicate glasses, by investigating the systematic variation of spectral response in reflectance on experimentally produced glasses. We focus not only on mafic or impact-like compositions, but we enlarge the variability of chemical compositions by including silica-rich compositions for different magmatic series. Our aims are: i) widening the existing databases for the interpretation of planetary rocks and ii) identify which features of glassy products are comparable with those of bulk rocks. We show that despite the difficulty to parameterize glassy materials since there are almost featureless and with a strong influence of grain size on the spectral parameters (albedo, slope, etc.), new and interesting information can be indeed derived. We anticipate that our results can aid in shedding light on possible silica-rich rocks cropping out on terrestrial bodies and, perhaps more importantly, the presented dataset can be used for deconvolution of spectra acquired in areas suspected to be volcanic in origin, where amorphous materials might reasonably play a central role in defining their spectral response.

2. Methodologies

2.1. Sample collection and preparation

Silicate glasses were synthesized starting from natural rocks collected on three different volcanic areas on Earth. In each area two rocks were collected, one representing the most mafic end-member (low-silica) and the other the most felsic end-member (high-silica). In detail, the two end-members from the Island of Vulcano Island (Aeolian Islands, Italy) are a shoshonite and a rhyolite. This sampling site was chosen because the Island of Vulcano is emplaced above an active subduction zone in the SE Tyrrhenian Sea, and the products of the area have a particularly alkaline character (De Astis et al. 1997, Rossi et al. 2017, Vetere et al. 2015a). Two other rocks, a basalt and a rhyolite, were collected in the Snake River Plain area (USA, hereon SRP). This area is emplaced in an intraplate tectonic setting, and the products of this area have a sub-alkaline character (Morgavi et al. 2013). Finally, two other rocks (a Hawaiite and a Benmoreite) were collected in the area of Mount Etna (Sicily). Products from this area show sub/alkaline to moderate alkaline character (Corsaro and Métrich 2016).

Each end-member was crushed, pulverized down to a grain size lower than 200µm, and molten at supra-liquidus temperature (1400 °C) for 4 hours in air. The obtained melts were quenched in air to glass and subsequently re-crushed and pulverized. This procedure was repeated twice in order to obtain homogeneous glassy materials (see Vetere et al. 2015b for further details). Glasses were finally crushed to powders with size ranging from 500 to 200 µm and then mixed to obtain a series of products with intermediate compositions. For the Vulcano series, three further intermediate samples were synthesized by mixing the shoshonite and the rhyolite end-members in different weight proportions. Hence, five glass compositions with variable shoshonite:rhyolite ratios of 100:0, 70:30, 50:50, 30:70, and 0:100 (hereafter referred to as S, S7, S5, S3, RS, respectively) were prepared. Similarly, six samples were synthesized by mixing basalt and rhyolite from the Snake River Plain in the following ratios: 100:0, 80:20, 60:40, 40:60, 20:80, and 0:100 (hereafter referred to as B, B8, B6, B4, B2, RB). Finally, three samples were synthesized by mixing the hawaiite and the benmoreite from Mount Etna in the following ratios: 100:0, 50:50, and 0:100 (hereafter referred to as M, M5, and V). Glasses were crushed and sieved down to <36 µm for the spectral analysis.

2.2. Chemical composition determination

Chemical compositions for all samples were determined at the Department of Earth- and Environmental Sciences, University of Munich LMU (Germany), with a Cameca SX100 electron microprobe analyzer (EMPA). Glass fragments were embedded in epoxy resin, polished, and then covered with a 13 nm carbon coating. Analyses were performed using an acceleration voltage of 15 kV and an electron beam current of 20 nA, with a defocused beam of 10 µm on the sample. Standards used for calibration were: orthoclase (Al, K), albite (Si, Na), wollastonite (Ca), periclase (Mg), ilmenite (Ti), iron(II) oxide (Fe), and chromium oxide (Cr). The chemical homogeneity of glasses was tested by performing five chemical analyses for each sample.

2.3. Iron speciation and SCFM determination

Ferrous–ferric ratio is dependent on the glass composition and may also depend on the conditions at which the melting process occurred. In this study, glasses were always prepared at air oxygen fugacity. The iron oxidation state determination was performed using a wet chemical micro-colorimetric method (Schuessler et al. 2008). 7–10 mg of glass chips were dissolved in concentrated HF with the addition of a solution of ammonium vanadate in 5M sulfuric acid. The released ferrous iron reacts with V^{5+} and forms V^{4+} and ferric iron (for details, see ref. Schuessler et al. 2008 and Vetere, Holtz, et al. 2014). After complete dissolution, boric acid was added to bind fluorine, and the pH value was increased by adding ammonium acetate so that Fe^{2+} was formed again. The concentration of bivalent iron was measured by means of spectroscopy after complexation with bipyridyl, using a 1 cm transmission cell in a UV/VIS spectrometer Shimadzu UV 1800. To measure

137 the total iron concentration (Fe_{tot}), hydroxylamine hydrochloride was added to the solution for the
138 reduction of Fe^{3+}. By combining this information with EPMA analyses, also the SCFM parameter was
139 calculated, as defined by Walter and Salisbury (1989), taking its name from the cations of the oxides
140 involved in its definition [i.e. $SiO_2/(SiO_2+CaO+FeO+MgO)$].

141 ### 2.4. Spectral characterization within VNIR

142 All the samples (in the form of <36 μm powders) were characterized at the C-Lab of the Institute for
143 Space Astrophysics and Planetology (IAPS-INAF) in Rome, Italy. The instrument we used is
144 described in detail in De Angelis et al. (2014), consisting of Field Spec-4 spectrometer, having a
145 detection spectral range of 0.35–2.5 μm. This range is covered by three separate detectors: the VIS
146 (0.35–1.0 μm), the SWIR1 (1.0–1.8 μm), and the SWIR2 (1.8–2.5 μm). Thus, the entire VNIR
147 spectrum is obtained by joining the spectra detected in each spectral sub-region. The spectral
148 sampling is 1 nm, whereas the spectral resolution is in the range of 3–8nm. A Quartz-Tungsten-
149 Halogen (QTH) lamp was used to illuminate the sample, with a spatial spot of about 5 mm. Optical
150 fibers were used both for illuminating and collecting the reflected light. The specimen (in our case
151 powdered glass) was placed on a three-stage sample holder, which allows for the movement of the
152 target along with the XYZ directions using three micrometric screws.
153 As for the quantitative determination of albedo and slope parameters, we have followed the
154 methodology shown in De Angelis et al. 2014: three slopes were determined, one in the visible region
155 (VIS slope, in the range between 0.5-0.8 μm), a second one in the near-infrared region (NIR slope in
156 the range between 1.2 and 1.8 μm), and a third one including the whole region (VNIR slope, in the
157 range 0.6 and 2.0 μm). As for albedo, two values were taken into account at 0.8 μm and 1.62 μm.
158 Moreover, we have taken into account a newly defined parameter: the spectral ratio of reflectance
159 values at 1.55 and 0.8 μm: $R_{1.55}/R_{0.8}$. These two wavelengths were chosen because no absorption
160 occurs in these zones.

161 ## 3. Results

162 ### 3.1. Chemical characterization

163 The chemical composition of all glasses is reported in Table 1, integrated with information about iron
164 speciation determination. It is observed how the procedure described above for the production of
165 compositional series successfully resulted in regular variations of the chemical content of all main
166 oxides. Results from chemical determinations are plotted in the Total Alkali vs Silica (TAS) diagram
167 in Figure 1 (LeBas et al. 1986). Here, the chemical variability of the products can be appreciated for
168 both the silica and the alkaline content. Noteworthy is the fact that the analyzed dataset within this
169 graph roughly covers more than the 90% of rock compositions cropping out on Earth (Best, 2013).

Here, datapoint colors are orange for SRP series, blue for Etna, and green for Vulcano series. Note that this color-coding will be maintained for each additional plot presented in this work.

3.2. Spectral characterization

All spectra acquired with FieldSpec 4 are reported in Figure 2, except for sample V from Etna series, which was found to experience incipient crystallization of magnetite (probably because of the occasional slow quench that might have been caused by laboratory bias, and therefore was not included for further analyses. Figure 2 is divided into three panels, each showing the set of spectra of a single series. For all three panels, the darker the colour, the most mafic is the composition. In general, spectra belonging to mafic products have lower reflectance and steeper slope, with the reflectance increasing and the slope flattening with increasing silica content and decreasing iron content. Vulcano products show generally higher reflectance and flatter slopes, even for the most mafic products. All spectra show three weak absorption bands, the two well-known absorption bands relative to Fe^{2+} absorption located at 1 and 2 μm (Hunt 1977, Cannon et al. 2017, Carli et al. 2016) and another small shoulder at ca. 0.45 μm, particularly evident only for the Vulcano series.

4. Discussion

4.1. Slope and albedo

Absorption features in VNIR reflectance are superimposed to a continuum, a background level of the reflectance spectra that is not constant with varying wavelengths. An exhaustive explanation of the nature of this phenomenon is not yet available. However, it is thought to be the combination of various processes, such as a larger absorption feature within the ultraviolet region, (Clark et al. 1999). For this reason, two of the spectral parameters that are usually taken into account when dealing with this kind of spectra are the albedo, which is the reflectance level at a certain wavelength, and the spectral slope. These two parameters can be retrieved from reflectance of planetary surface, even from low-resolution spectral characterization. These parameters are observed to be dependent not only on chemical composition but also on physical features, such as the grain size, and the observational conditions, such as the phase, incidence, and emission angles. The dependence of slope and albedo on grain size has been studied for rocks (De Angelis et al. 2014) and glasses (Carli, et al. 2016). As mentioned in section 2.4, we have characterized the spectra quantitatively with albedos and slopes as defined by De Angelis et al. 2014, and, moreover, we have introduced a novel parameter: $R_{1.55}/R_{0.8}$. These values are reported in Table 2 and plotted as a function of three different chemical parameters in Figure 3 and 4: i) total iron (taken into account as FeO) as determined by EPMA analyses, ii) ferric iron (Fe_2O_3), and iii) SCFM parameter. SCFM is a chemical parameter introduced by Walter and Salisbury 1989. It is typically used for spectroscopic characterization and describes the degree of

evolution (in the petrological jargon) of a given composition. The more mafic and primitive the composition, the closer SCFM will be to zero (although for bulk igneous natural compositions, it is never lower than 0.5). The more felsic and evolved the compositions, the closer SCFM will be to 1. The latter is the case of quartz or pure silica. Therefore, SCFM is a parameter that accounts for both chemical evolution of igneous products (SiO_2 content) and for iron content and speciation (iron in SCFM is accounted only in its ferrous form, FeO). By observing the trends of slopes changing with chemical composition three observations can be made:

i) regarding VIS slopes (Figure 3 a, b, and c) of SRP series, SRP and Etna values are decreasing with increasing iron (i.e. decreasing SCFM), whereas the trend is reversed for Vulcano alkaline series. Data-points appear more scattered in those plots where the slope is shown as a function of iron content. When observing the VIS slope-SCFM plot, data-points are better distributed along a line, with S7 and S5 still within the trends of the others series, and S3 and RS outlying the trend; ii) as for NIR slope (Figure 4 d, e and f), it appears to increase with increasing iron content and decreasing SCFM, except for mafic alkaline products, for which the trend is reversed; iii) regarding the slope within the entire VNIR range (Figure 3 g, h, i) datapoints of slopes are scattered around 0.021 ± 0.02, again with the exception of Vulcano series, mainly driven by the above-mentioned trend in the visible region, that makes the slope of the whole series to drop down to ca. 0.09. For VIS and NIR slopes, we have observed how value variation is substantially different, depending on whether we are observing sub-alkaline or alkaline series. For the sub-alkaline series, the VIS slope increases from mafic towards felsic compositions, as the iron content decreases. This trend is inverted for alkaline series: in this case, VIS slope drops from mafic to felsic compositions, and this trend is progressively more evident as the compositions become more evolved. As for the NIR slope, generally, it is steeper for mafic compositions and flatter for felsic compositions, although alkaline mafic compositions tend to show flatter slopes. The influence of iron-poor and alkaline-rich composition on the spectral response of silicate glasses within VNIR has already been observed by Cannon et al. 2017, who investigated Mercury-like mafic compositions. However, in this study, we had a closer look at a wider range of chemical compositions, and we have confirmed the complexity of this phenomenon.

For what concerns the variation of albedo as a function of SCFM, it appears more uniform, as it is possible to observe in Figure 4. Generally, both for NIR and VIS, albedo is decreasing with increasing iron content, and therefore the global reflectivity is higher moving from mafic compositions towards felsic compositions. However, the general trend differs when different parameters are taken into account. When the albedo is plotted as a function of total iron as FeO, trends are slightly different for alkaline and sub-alkaline products, the latter decreasing more rapidly in albedo as iron content increases. When plotting albedo and Fe^{3+}, data collapse into a single trend, and this phenomenon is even more pronounced if albedo values are plotted vs. SCFM. In general, we can say that the larger SCFM, the higher is the albedo in all the VNIR range. The same observations can be made when

observing parametrization with spectral ratio $R_{1.55}/R_{0.8}$ (Figure 4 g, h, i), although this parameter seems to make the data-points to collapse in a single trend for all the three chemical parameters taken into account.

4.2. Band centres and absorption areas

Absorptions bands in VNIR spectra of materials occur for two reasons: electronic processes or molecular vibrations. Among the former, there are crystal field effects, occurring in the transitional elements with inner unfilled electron shells; the crystalline field modifies the degeneration of atomic orbitals allowing the electronic transitions between shells. For what concern minerals and rocks, Fe is by far the most abundant transitional element, and therefore the observation of crystal field absorptions of Fe in the VNIR is diagnostic for mineralogy since this absorption varies among different mineral phases. Another electronic absorption process is the so-called charge transfer absorption, caused by interelement transitions of electrons between ions or between ions and ligands; this is also often diagnostic for mineral phases (Hunt 1977, Burns 1993, Clark et al. 1999).

On the other hand, vibrational processes occur when the bonds in IR active molecules or functional groups vibrate. Bonds behave like springs, and a molecule can vibrate or rotate, although rotational modes occur in gas or liquid phases. This phenomenon occurs within the VNIR region for many bonds involving C, O, and OH, and therefore it can be diagnostic for phyllosilicates, carbonates, or water-bearing phases (Ferrari et al. 2019). Due to the lack of a regular crystalline structure, absorption bands are very weak for glasses. However, in the VNIR region, literature reports four absorption phenomena (Hunt 1977, Burns 1993, Clark et al. 1999, Cannon et al. 2017). The most evident are two absorption bands at ca. 1.05 µm and 1.9 µm, relative to crystal field absorptions of octahedral Fe^{2+}, and tetrahedral Fe^{2+}, respectively. Two other absorption phenomena can be attributed to oxygen-metal charge transfer (at the boundary with the ultraviolet region) and heterovalent charge transfer absorptions Fe^{2+}-Fe^{3+} around 0.8 µm (Bell et al. 1976). For our set of spectra, bands at ca. 1.1 µm and 1.9 µm are evident, whereas another little absorption featureis detectable at ca. 0.5-0.6 µm for alkaline and very felsic products. To refine and quantitatively describe the absorption phenomena within this range, data analysis was performed using the Origin © software. Smoothing of spectra was performed by applying a Fast Fourier Transform filter (FFT filter) on a window consisting of 50 to 100 data-points, depending on each spectrum's characteristics. FFT filter method is particularly suitable for noises whose frequency is higher than the frequency of the true signal. For our set of spectra, this occurs towards the upper limit of the spectral range, between 2.2 and 2.5 µm. Continuum removal was performed by subtracting baseline to each spectrum considered as 1-Reflectance. The baseline was designed individually for each spectrum by selecting anchoring points in the ranges where no absorptions were observed (ca. < 0.8 µm, 1.5 and > 2.3 µm) and by connecting these points with a spline function. The different steps of the described processes can be visualized in Figure 5.

Finally, peak fitting was performed on the two bands of absorption at ca. 1.15 and 1.9μm. Indeed, by taking into consideration the spectra as 1-Reflectance, the typical two local reflectance minimums became two peaks that were possible to be deconvoluted to two Gaussian functions, through the option PeakFit Pro of the Origin software. Peak centers were picked manually, and then let free to oscillate during the fit process. Table 3 reports all the parameters resulting from the fitting process, whereas Figure 6 reports band centers and area percentage of both absorptions bands, plotted with total iron content.

Band centres (Figure 6a) generally slightly shift with iron content and there is no clear difference between different series. There is a slight shift (up to 0.01 μm) towards higher wavelengths for extremely felsic (low-iron) compositions, but this is indeed quite small and, if considered as one series all together, the absorption relative to Fe^{2+} crystal field octahedral absorption is averagely positioned at 1.15 μm (covering a span between 1.12 and 1.18 μm), while the one relative to tetrahedral absorption is averagely positioned at 1.93 μm (covering a span between 1.89 and 1.99 μm). Carli, et al. 2016 have observed how, for glasses having the same composition and different granulometry, the shift of centers of absorption is apparent, and it is not visible after continuum removal. However, in the mentioned study, only mafic compositions were investigated, as in the vast majority of planetary-related studies. Our set of spectra is also presenting a variation of the slope with changing chemical composition that creates an apparent shift of the centers. After being treated by smoothing, continuum removal, and having performed quantitative analyses, we conclude that the observed weak shift is an artifact, and we can state that no shift in the band centers is present for silicate glasses. In Figure 6b it is also reported the relationship between the absorption areas of each centre (expressed as a percentage over the total for both absorption bands) and, again, the total iron content. Even if some scatter is visible, there is a general trend: with increasing iron, absorption linked to tetrahedral Fe^{2+} increases, whereas octahedral Fe^{2+} decreases. This phenomenon looks stronger for Vulcano alkaline series rather than for SRP sub-alkaline series, whereas the Etna series looks too restricted to make detailed considerations. An interpretation of this phenomenon could be related to the fact that, with increasing iron content, we are decreasing silica content (Table 1). This way, the tetrahedral network (mainly composed of SiO^{2+} tetrahedral cells) becomes less polymerized, so that iron Fe^{2+} is freer to occupy these slots, given also the fact that a lower viscosity results in larger mobility of the elements within the melt. This trend is considerably stronger for alkaline series, because, as already known (Mysen and Richet 2005), alkalis act as charge balancers and trigger other elements (such as iron) to act as network former in the tetrahedral network.

Conclusions

Three different series of glasses, for a total of 15 samples, have been produced from natural rocks under controlled conditions. Fine powders of such glasses were characterized spectroscopically in reflectance in the Visible and Near-Infrared region (VNIR). Such investigation revealed that

i) Extremely fine powders of silicate glasses have always positive slopes. For the sub-alkaline series, glasses presenting mafic composition have a steeper slope if compared to felsic composition, this trend is inverted for alkaline series, which have generally a flatter aspect. There is therefore a fundamental difference in the variation of slopes between alkaline and sub-alkaline products.

ii) For such silicate glasses powders, the variation of albedo is similar for all series, with mafic glasses being always darker in comparison with felsic glasses. If compared to SCFM parameter, the albedo of all investigated glasses clusters into a close-to-unique trend. However, according to our analysis, the best parameter to describe iron content and SCFM is the one proposed for the first time here: $R_{1.55}/R_{0.8}$

iii) Silicate glasses having widely different chemical composition are characterized by two weak absorptions, at 1.15 µm and 1.93 µm. A small shoulder at ca. 0.5 µm is observable for felsic glasses, in particular for alkaline series. The relative area of absorption at 1.1 µm increases moving from mafic to felsic products (and therefore is inversely proportional to iron content), whereas band depth absorption at 1.9 µm decreases moving from mafic towards felsic composition (and therefore directly proportional to iron content).

In order to suggest possible applications of this study for the interpretation of planetary data, we highlight that VIS slopes analyses can be useful for distinguishing sub-alkaline and alkaline products for felsic composition, whereas NIR and VNIR slope analyses are more helpful for distinguishing sub-alkaline and alkaline products for mafic composition. On the other hand, albedo is certainly a good marker for the degree of evolution of chemical composition, in particular when expressed as SCFM. The novel parameter $R_{1.55}/R_{0.8}$ appears to be the best one to determine both the abundance of iron and the SCFM parameter.

It has to be noted that this study concerned samples having the same, very fine, grain size (<36 µm), but grain size has been observed as having a large influence on slopes and albedos. Although therefore, additional efforts must be done to include in the analysis also these variables, this study represents a step forward in the knowledge of the possible factors influencing spectral response within the VNIR range of glasses. This integrates the state of the knowledge on the spectral response of geologically relevant material, especially for what concerns igneous products, of which glassy or hypohyaline products represent the most plausible occurrences.

The new presented dataset can be helpful in the context of future missions aimed at understanding the nature of rocks on other planets and, especially, for the important upcoming mission ExoMars, by ESA/ROSCOSMOS (Vago et al., 2017). Such a mission comprises different launches and, in 2022, it

will deliver a European rover, Rosalind Franklin, and a Russian surface platform, Kazachok on the surface of Mars. In particular, Rosalind Franklin will carry nine different instruments for the physical and chemical *in situ* analysis of the Martian surface. This rover will be able to drill 1x3 cm rock cores from up to 2 meters depth, with a drill integrated with the Mars Multispectral Imager for Subsurface Studies (Ma_MISS) to constrain mineralogy and rock formation dynamics by characterizing the spectra in the visible and near-infrared (De Sanctis et al., 2017). Data presented within this study will be fundamental to interpret possible volcanic ash occurrences on future missions to Mars.

Acknowledgements

We acknowledge the support of ASI under the ASI-UniPGagreement 2019-2-HH.0. A.P. would like to thank P. Baldini for technical support.

References

Adams, J. B. (1975). "Interpretation of visible and near-infrared diffuse reflectance spectra of pyroxenes and other rock-forming minerals". In: Infrared and Raman spectroscopy of lunar and terrestrial minerals, pp. 91–116.

Adams, J. B. and A. L. Filice (1967). "Spectral reflectance 0.4 to 2.0 microns of silicate rock powders". In: Journal of Geophysical Research 72.22, pp. 5705–5715.

Anbazhagan, S. and S. Arivazhagan. (2010). "Reflectance spectra of analog anorthosites: Implications for lunar high- land mapping". In: Planetary and Space Science 58.5, pp. 752–760.

Bell, P. M., H. K. Mao, and R. A. Weeks (1976). "Optical spectra and electron paramagnetic resonance of lunar and synthetic glasses-A study of the effects of controlled atmosphere, composition, and temperature". In: Lunar and Planetary Science Conference Proceedings. Vol. 7, pp. 2543–2559.

Best, M. G. (2013). Igneous and metamorphic petrology. John Wiley & Sons.

Bishop, J. L., R. T. Schelble, C. P. McKay, A. J. Brown, and K. A. Perry (2011). "Carbonate rocks in the Mojave Desert as an analogue for Martian carbonates". In: International Journal of Astrobiology 10.4, p. 349.

Boynton, W. V., Ming, D. W., Kounaves, S. P., Young, S. M. M., Arvidson, R. E., Hecht, M. H., ... & Morris, R. V. (2009). Evidence for calcium carbonate at the Mars Phoenix landing site. Science, 325(5936), 61-64.

Burns, R. G. (1993). Mineralogical applications of crystal field theory. Vol. 5. Cambridge university press.

Cannon, K. M., J. F. Mustard, S. W. Parman, E. C. Sklute, M. Darby Dyar, and R. F. Cooper (2017). "Spectral properties of Martian and other planetary glasses and their detection in remotely sensed data". In: Journal of Geophysical Research: Planets 122.1, pp. 249–268.

Carli, C., M. Ciarniello, F. Capaccioni, G. Serventi, and M. Sgavetti (2014). "Spectral variability of plagioclase– mafic mixtures (2): Investigation of the optical constant and retrieved mineral abundance dependence on particle size distribution". In: Icarus 235, pp. 207–219.

Carli, C., T. L. Roush, G. Pedrazzi, and F. Capaccioni (2016). "Visible and Near-Infrared (VNIR) reflectance spectroscopy of glassy igneous material: Spectral variation, retrieving optical constants and particle sizes by Hapke model". In: Icarus 266, pp. 267–278.

Clark, R. N. (1999). Spectroscopy of rocks and minerals, and principles of spectroscopy. Manual of remote sensing, 3(3-58), 2-2.Cloutis, E. A., M. J. Gaffey, D. G. W. Smith, and R. J. Lambert (1990). “Reflectance spectra of glass-bearing mafic silicate mixtures and spectral deconvolution procedures”. In: Icarus 86.2, pp. 383–401.

Cloutis, E. A., D. H., D. M. Applin, J. P. Mann, and S.A. Mertzman (2018). “Raman and reflectance spectroscopy of serpentinites and related hydrated silicates: effects of physical properties and observational parameters, and implications for detection and characterization on Mars”. In: Planetary and Space Science 159, pp. 66–83.

Cloutis, E. A., T. Hiroi, M. J. Gaffey, C. M. O’D. Alexander, and P. Mann (2011). “Spectral reflectance properties of carbonaceous chondrites: 1. CI chondrites”. In: Icarus 212.1, pp. 180–209.

Cloutis, E. A., M. R. M. Izawa, and P. Beck (2018). “Reflectance spectroscopy of chondrites”. In: Primitive Meteorites and Asteroids. Elsevier, pp. 273–343.

Corsaro, R. A. and N. Métrich (2016). “Chemical heterogeneity of Mt. Etna magmas in the last 15 ka. Inferences on their mantle sources”. In: Lithos 252, pp. 123–134.

Crown, D. A. and C. M. Pieters (1987). “Spectral properties of plagioclase and pyroxene mixtures and the interpretation of lunar soil spectra”. In: Icarus 72.3, pp. 492–506.

De Angelis, S., M. C. De Sanctis, E. Ammannito, C. Carli, T. Di Iorio, and F. Altieri (2014). “The Ma_Miss instrument performance, I: Analysis of rocks powders by Martian VNIR spectrometer”. In: Planetary and Space Science 101, pp. 89–107.

De Angelis, S., Carli, C., Tosi, F., Beck, P., Schmitt, B., Piccioni, G., ... & Philippe, S. (2017). Temperature-dependent VNIR spectroscopy of hydrated Mg-sulfates. Icarus, 100(281), 444-458.De Astis, G., L. La Volpe, A. Peccerillo, and L. Civetta (1997). “Volcanological and petrological evolution of Vulcano island (Aeolian Arc, southern Tyrrhenian Sea)”. In: Journal of Geophysical Research: Solid Earth 102.B4, pp. 8021–8050.

Evans, D. L., T. G. Farr, and J. B. Adams (1982). “Spectral reflectance of weathered terrestrial and Martian surfaces”. In: Lunar and Planetary Science Conference Proceedings. Vol. 12, pp. 1473–1479.

Ferrari, M., S. De Angelis, M. C. De Sanctis, E. Ammannito, S. Stefani, and G. Piccioni (2019). “Reflectance spectroscopy of ammonium-bearing phyllosilicates”. In: Icarus 321, pp. 522–530.

Gaffey, M. J. (1976). “Spectral reflectance characteristics of the meteorite classes”. In: Journal of Geophysical Research 81.5, pp. 905–920.

Gendrin, A., Mangold, N., Bibring, J. P., Langevin, Y., Gondet, B., Poulet, F., ... & LeMouélic, S. (2005). Sulfates in Martian layered terrains: the OMEGA/Mars Express view. Science, 307(5715), 1587-1591.Harloff, J. and G. Arnold (2001). “Near-infrared reflectance spectroscopy of bulk analog materials for planetary crust”. In: Planetary and Space Science 49.2, pp. 191–211.

Harner, P.-L. and M. S. Gilmore (2015). “Visible–near infrared spectra of hydrous carbonates, with impli- cations for the detection of carbonates in hyperspectral data of Mars”. In: Icarus 250, pp. 204–214.

Hiroi, T., Kaiden, H., Misawa, K., Kojima, H., Uemoto, K., Ohtake, M., ... & Shih, C. Y. (2012, March). Diversity in the visible-NIR absorption band characteristics of lunar and asteroidal plagioclase. In Lunar and Planetary Science Conference (No. 1659, p. 1168).

Hunt, G. R. (1977). “Spectral signatures of particulate minerals in the visible and near infrared”. In: Geophysics 42.3, pp. 501–513.

Isaacson, P. J, R. L. Klima, J. M. Sunshine, L. C. Cheek, C. M Pieters, T. Hiroi, M. D. Dyar, M. Lane, and J. L. Bishop (2014). “Visible to near-infrared optical properties of pure synthetic olivine across the olivine solid solution”. In: American Mineralogist 99.2-3, pp. 467–478.

Kargel, J. S., Kirk, R. L., Fegley Jr, B., & Treiman, A. H. (1994). Carbonate-sulfate volcanism on Venus?. Icarus, 112(1), 219-252.

Klima, R. L., C. M. Pieters, and M. D. Dyar (2008). "Characterization of the 1.2 μm M1 pyroxene band: Ex- tracting cooling history from near-IR spectra of pyroxenes and pyroxene-dominated rocks". In: Meteoritics & Planetary Science 43.10, pp. 1591–1604.

Klima, R. L, C. M. Pieters, and M. D. Dyar (2009). "Pyroxene spectroscopy: Probing composition and thermal history of the lunar surface". In: LPI, p. 2155.

LeBas, M. J., R. W. Le Maitre, A. Streckeisen, B. Zanettin, and IUGS Subcommission on the Systematics of Igneous Rocks (1986). "A chemical classification of volcanic rocks based on the total alkali-silica diagram". In: Journal of petrology 27.3, pp. 745–750.

Markus, K., L. Moroz, G. Arnold, D. Henckel, H. Hiesinger, Rohrbach, and S. Klemme (2018). "Reflectance spectra of synthetic Fe-free ortho-and clinoenstatites in the UV/VIS/IR and implications for remote sensing detection of Fe-free pyroxenes on planetary surfaces". In: Planetary and Space Science 159, pp. 43–55.

Minitti, M. E., J. F. Mustard, and M. J. Rutherford (2002). "Effects of glass content and oxidation on the spectra of SNC-like basalts: Applications to Mars remote sensing". In: Journal of Geophysical Research: Planets 107.E5, pp. 6-1-6–14.

Mølholt, T. E, H. P. Gunnlaugsson, J. P. Merrison, R. V. Morris, and P. Nørnberg (2008). "Mössbauer and VNIR study of dust generated from olivine basalt: application to Mars". In: Hyperfine Interactions 186.1-3, pp. 127–133.

Morgavi, D., D. Perugini, C. P. De Campos, W. Ertl-Ingrisch, Y. Lavallée, L. Morgan, and D. B. Dingwell (2013). "Interactions between rhyolitic and basaltic melts unraveled by chaotic mixing ex- periments". In: Chemical Geology 346, pp. 199–212.

Moroz, L.V. et al. (2009). "Spectral properties of simulated impact glasses produced from martian soil analogue JSC Mars-1". In: Icarus 202.1, pp. 336–353. issn: 0019-1035.

Morris, R. V., Ruff, S. W., Gellert, R., Ming, D. W., Arvidson, R. E., Clark, B. C., ... & Squyres, S. W. (2010). Identification of carbonate-rich outcrops on Mars by the Spirit rover. Science, 329(5990), 421-424.Murchie, S., Roach, L., Seelos, F., Milliken, R., Mustard, J., Arvidson, R., ... & Morris, R. (2009). Evidence for the origin of layered deposits in Candor Chasma, Mars, from mineral composition and hydrologic modeling. Journal of Geophysical Research: Planets, 114(E2).Mustard, J. F., F. Poulet, A. Gendrin, J.-P. Bibring, Y. Langevin, B. Gondet, N. Mangold, G. Bellucci, and F. Altieri (2005). "Olivine and pyroxene diversity in the crust of Mars". In: Science 307.5715, pp. 1594–1597.

Mysen, B. O. and P. Richet (2005). Silicate glasses and melts: properties and structure. Vol. 10. Elsevier. Penttilä, Antti, Timo Väisänen, Johannes Markkanen, Julia Martikainen, Tomáš Kohout, Gorden Videen, and

K. Muinonen (2020). "Rigorous light-scattering simulations of nanophase iron space-weathering effects on reflectance spectra of olivine grains". In: Icarus, p. 113727.

Pompilio, L., M. Sgavetti, and G. Pedrazzi (2007). "Visible and near-infrared reflectance spectroscopy of pyroxene-bearing rocks: New constraints for understanding planetary surface compositions". In: Journal of Geophysical Research: Planets 112.E1.

Poulet, F., J.-P. Bibring, J. F Mustard, A. Gendrin, N. Mangold, Y. Langevin, RE Arvidson, B Gondet, and C Gomez (2005). "Phyllosilicates on Mars and implications for early Martian climate". In: Nature 438.7068, pp. 623–627.

Rossi, S., M. Petrelli, D. Morgavi, D. Gonzalez-Garcia, L. A. Fischer, F. Vetere, and D. Perugini (2017). "Exponential decay of concentration variance during magma mixing: Robustness of a volcanic chronometer and implications for the homogenization of chemical heterogeneities in magmatic systems". In: Lithos 286, pp. 396–407.

Schuessler, J. A, R. E Botcharnikov, H. Behrens, V. Misiti, and C. Freda (2008). "Amorphous Materials: Properties, structure, and Durability: Oxidation state of iron in hydrous phono-tephritic melts". In: American Mineralogist 93.10, pp. 1493–1504.

Serventi, G., C. Carli, M. Sgavetti, M. Ciarniello, F. Capaccioni, and G. Pedrazzi (2013). "Spectral variability of plagioclase–mafic mixtures (1): Effects of chemistry and modal abundance in reflectance spectra of rocks and mineral mixtures". In: Icarus 226.1, pp. 282–298.

Sgavetti, M., L. Pompilio, and S. Meli (2006). "Reflectance spectroscopy (0.3–2.5 μm) at various scales for bulk-rock identification". In: Geosphere 2.3, pp. 142–160.

Singer, R. B. (1982). "Visible and near-IR spectral reflectance of geologically important materials: A short review".

Tompkins, S. and C. M. Pieters (2010). "Spectral characteristics of lunar impact melts and inferred miner- alogy". In: Meteoritics & Planetary Science 45.7, pp. 1152–1169.

Vago, J. L., Westall, F., Coates, A. J., Jaumann, R., Korablev, O., Ciarletti, V., ... & Carreau, C. (2017). Habitability on early Mars and the search for biosignatures with the ExoMars Rover. Astrobiology, 17(6-7), 471-510.

Vetere, F., F. Holtz, H. Behrens, R. E Botcharnikov, and S. Fanara (2014). "The effect of alkalis and polymerization on the solubility of H 2 O and CO 2 in alkali-rich silicate melts". In: Contributions to Mineralogy and Petrology 167.5, p. 1014.

Vetere, F., M. Petrelli, D. Morgavi, and D. Perugini (2015a). "Dynamics and time evolution of a shallow plumbing system: The 1739 and 1888–90 eruptions, Vulcano Island, Italy". In: Journal of Volcanology and Geothermal Research 306, pp. 74–82.

Vetere, F., G. Iezzi, H. Behrens, F. Holtz, G. Ventura, V. Misiti, A.Cavallo, S. Mollo, and M. Dietrich (2015b). "Glass forming ability and crystallisation behaviour of sub-alkaline silicate melts". In: Earth-science reviews 150, pp. 25–44.

Walter, L. S. and J. W. Salisbury (1989). "Spectral characterization of igneous rocks in the 8-to 12-μm region". In: Journal of Geophysical Research: Solid Earth 94.B7, pp. 9203–9213.

Wells, E. D. and B. Hapke (1977). "Lunar Soil: Iron and Titanium Bands in the Glass Fraction". In: Science 195.4282, pp. 977–979. issn: 0036-8075.

Wray, J. J., S. L. Murchie, B. L. Ehlmann, R. E. Milliken, J. L. Bishop, K. D. Seelos, E. Z. Noe Dobrea, J. F. Mustard, and S. W. Squyres (2011). "Orbital evidence for iron or calcium carbonates on Mars". In: EPSC-DPS Jt. Meet.

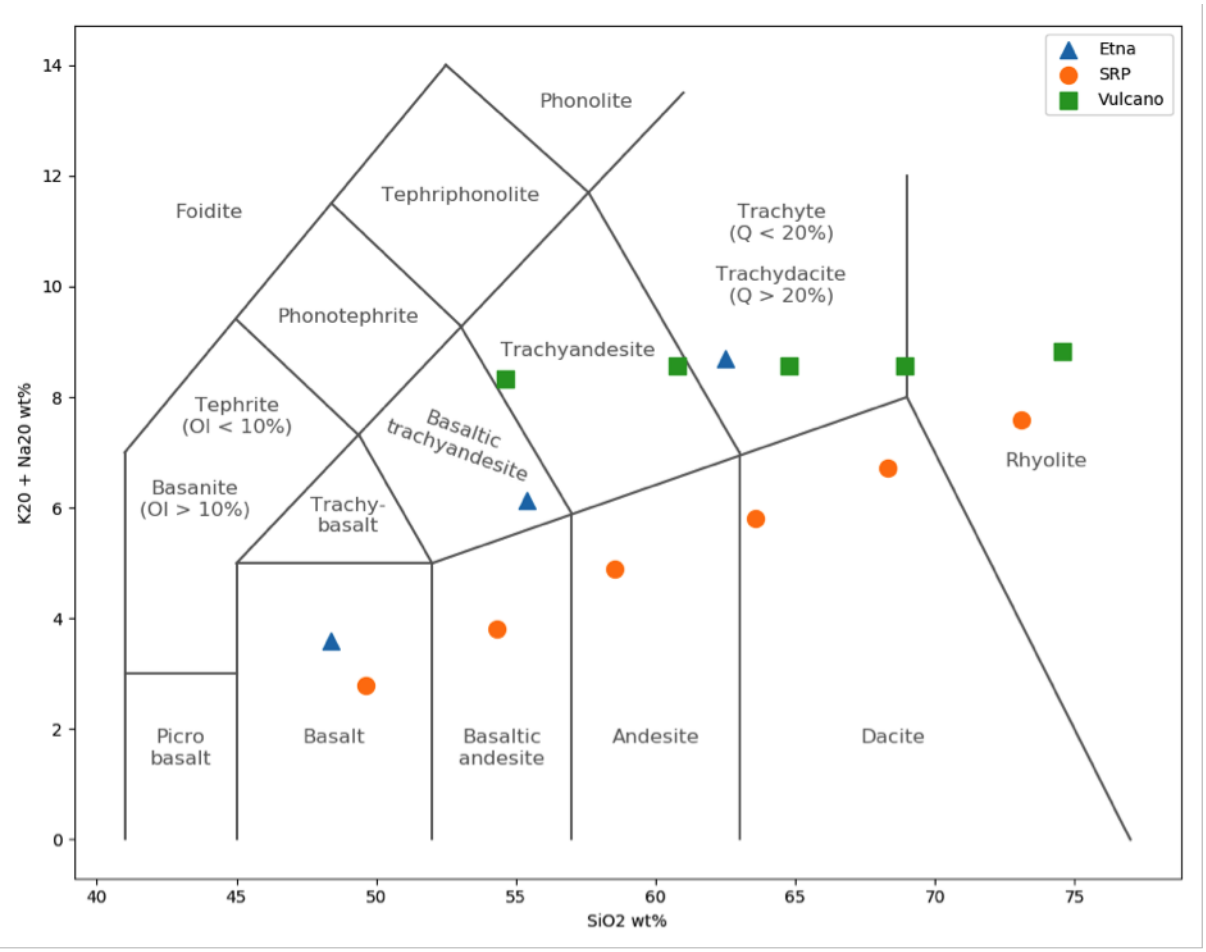

Figure 1: *TAS diagram reporting chemical composition of all analysed samples*

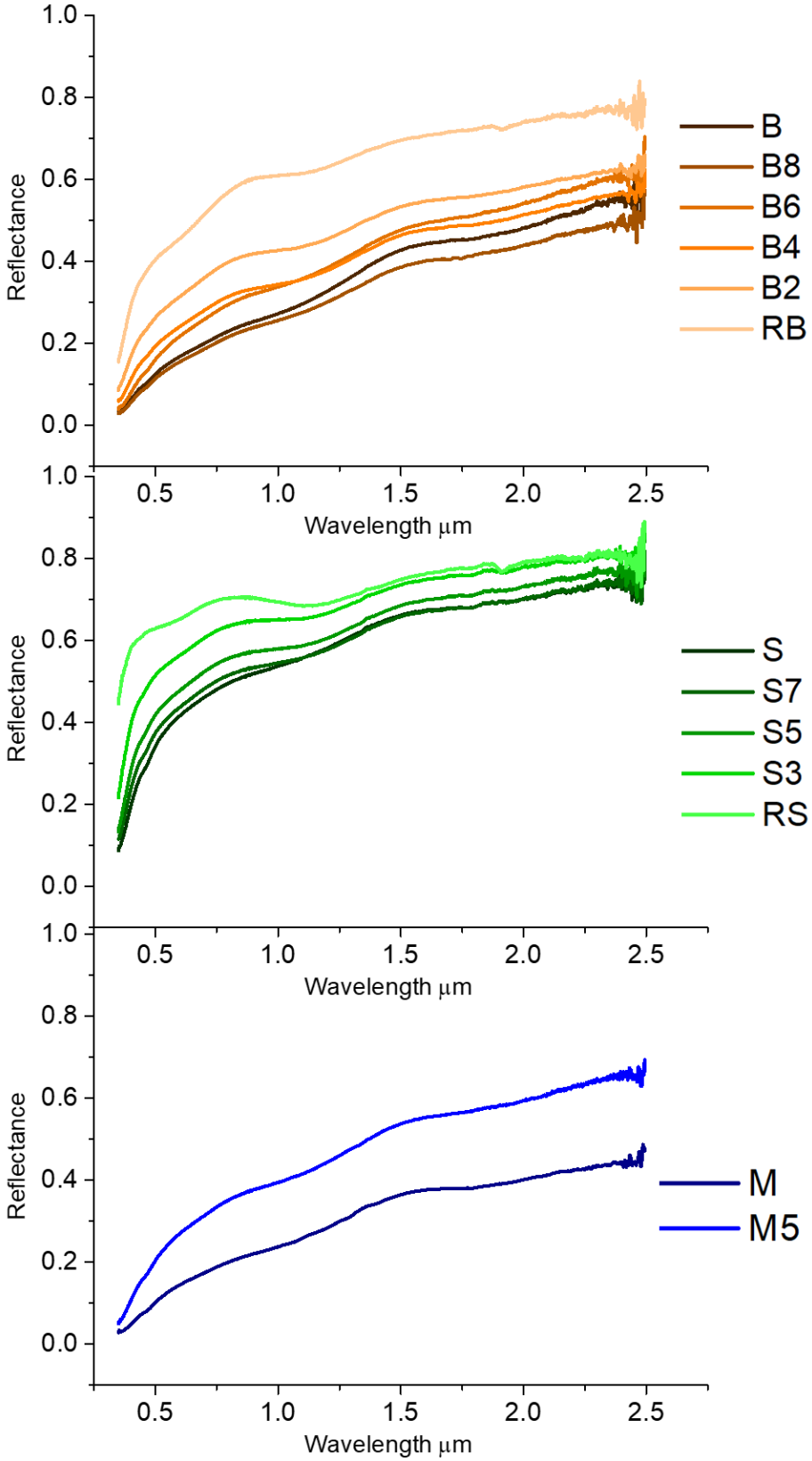

Figure 2: *Spectral dataset for the three series: SRP (above, orange), Vulcano (middle, green), Etna (bottom, blue). Darker colour in the graph indicates more mafic, iron-rich composition.*

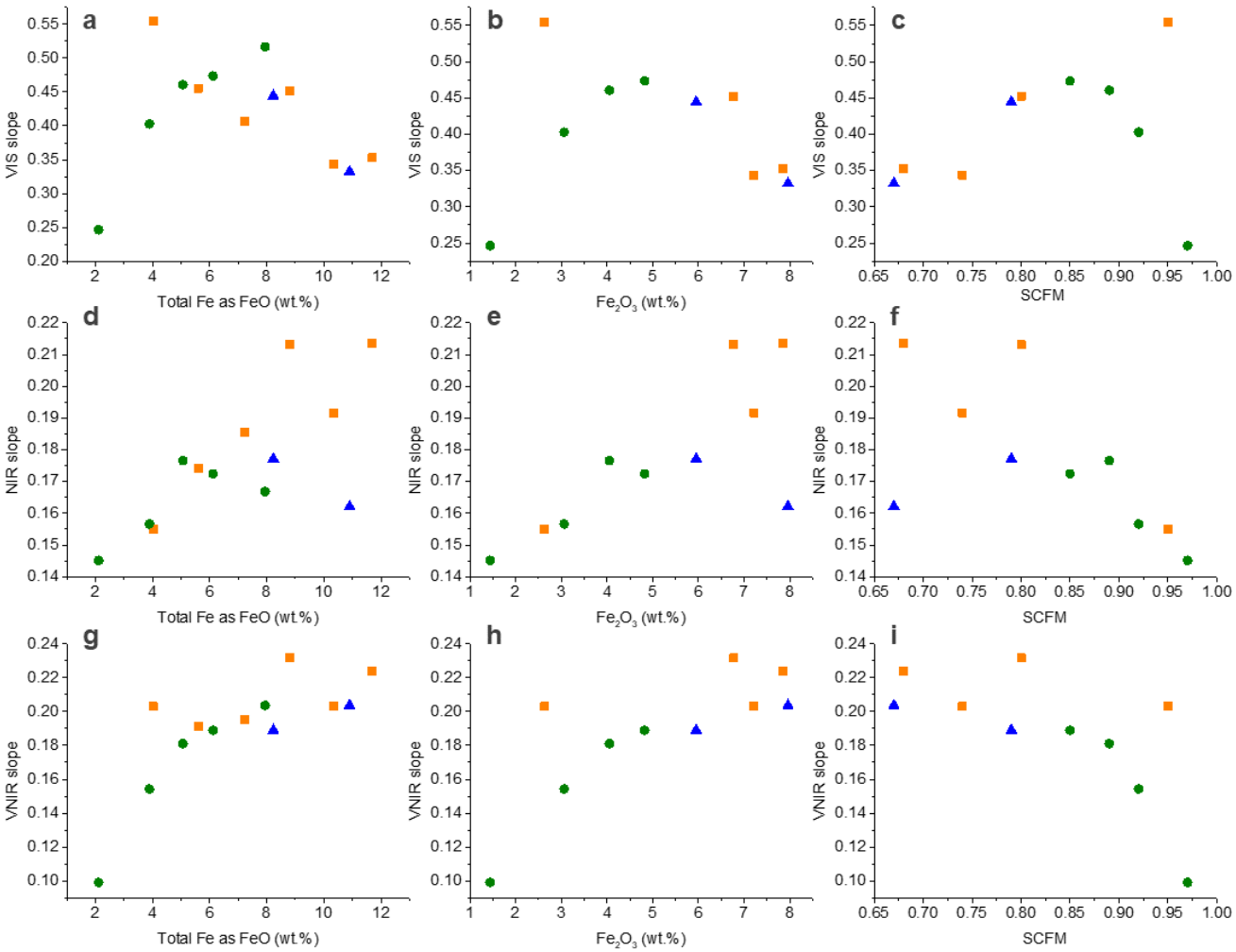

Figure 3: *Slopes of spectra in Figure 2 plotted versus different chemical parameters: total iron content, ferric iron content and SCFM. Orange squares represent SRP, green circles represent Vulcano and blue triangles represent Etna samples. Slopes σ are reported in Table 2, showing how vertical error bars would be smaller than symbols in this picture.*

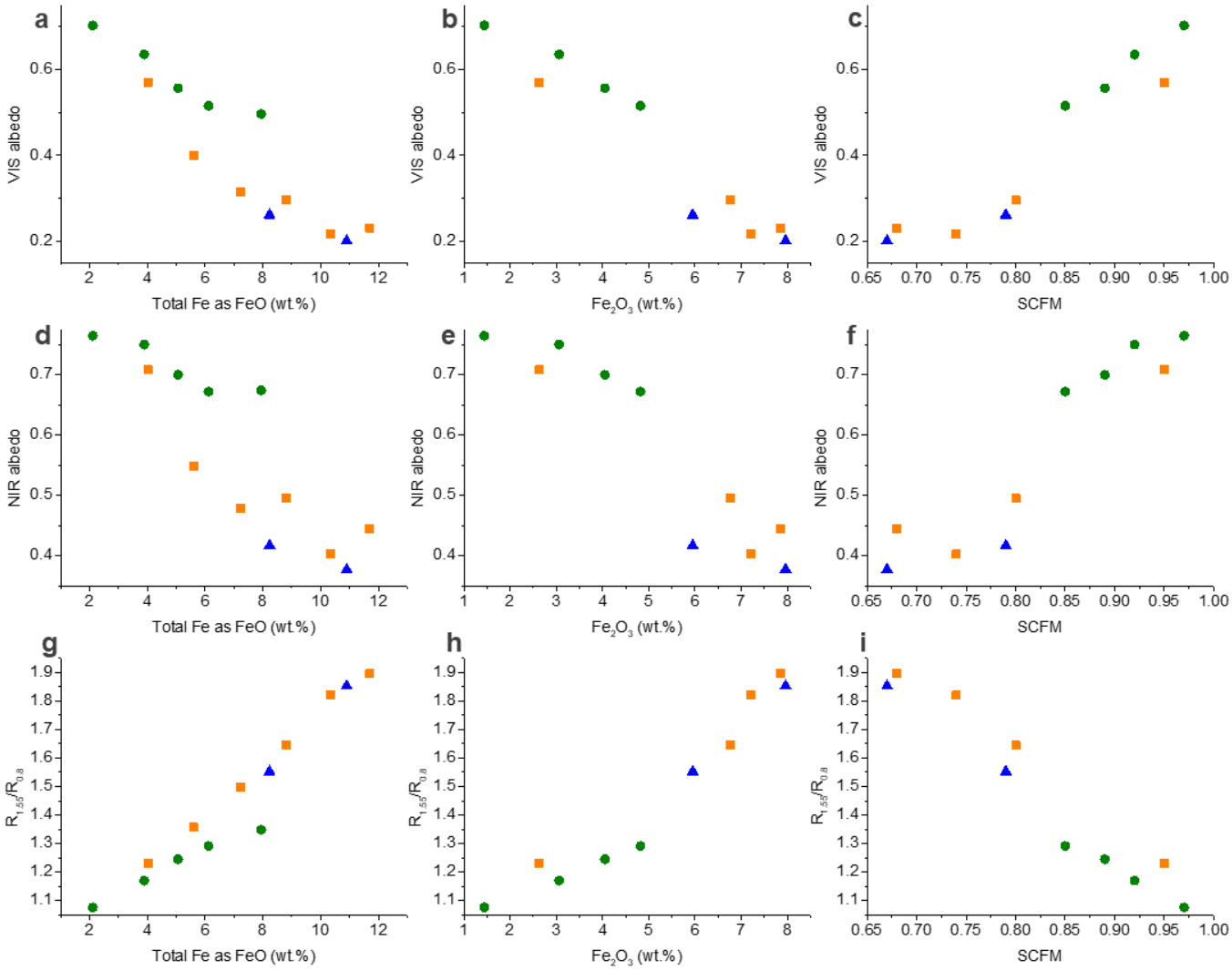

Figure 4: *Albedos and spectra ratio $R_{1.55}/R_{0.8}$ of spectra in Figure 2 plotted versus different chemical parameters: total iron content, ferric iron content and SCFM. Orange squares represent SRP, green circles represent Vulcano and blue triangles represent Etna samples. Values σ are reported in Table 2, showing how vertical error bars would be smaller than symbols in this picture.*

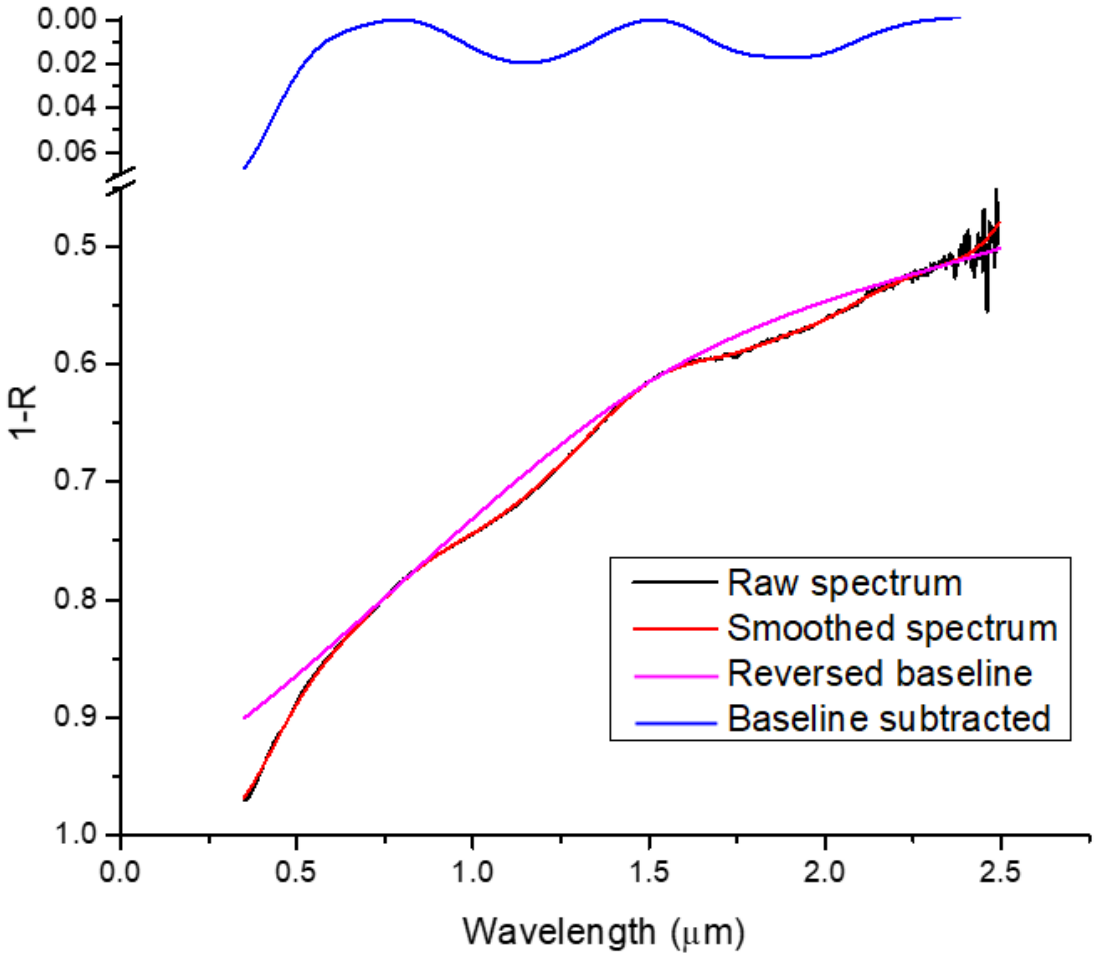

Figure 5: *Example of the refinement passages performed from starting from the raw spectrum (black line) which is smoothed (red line). On the smoothed spectrum it is applied a reversed baseline (pink line) to obtain continuum-subtracted spectrum (blue line)*

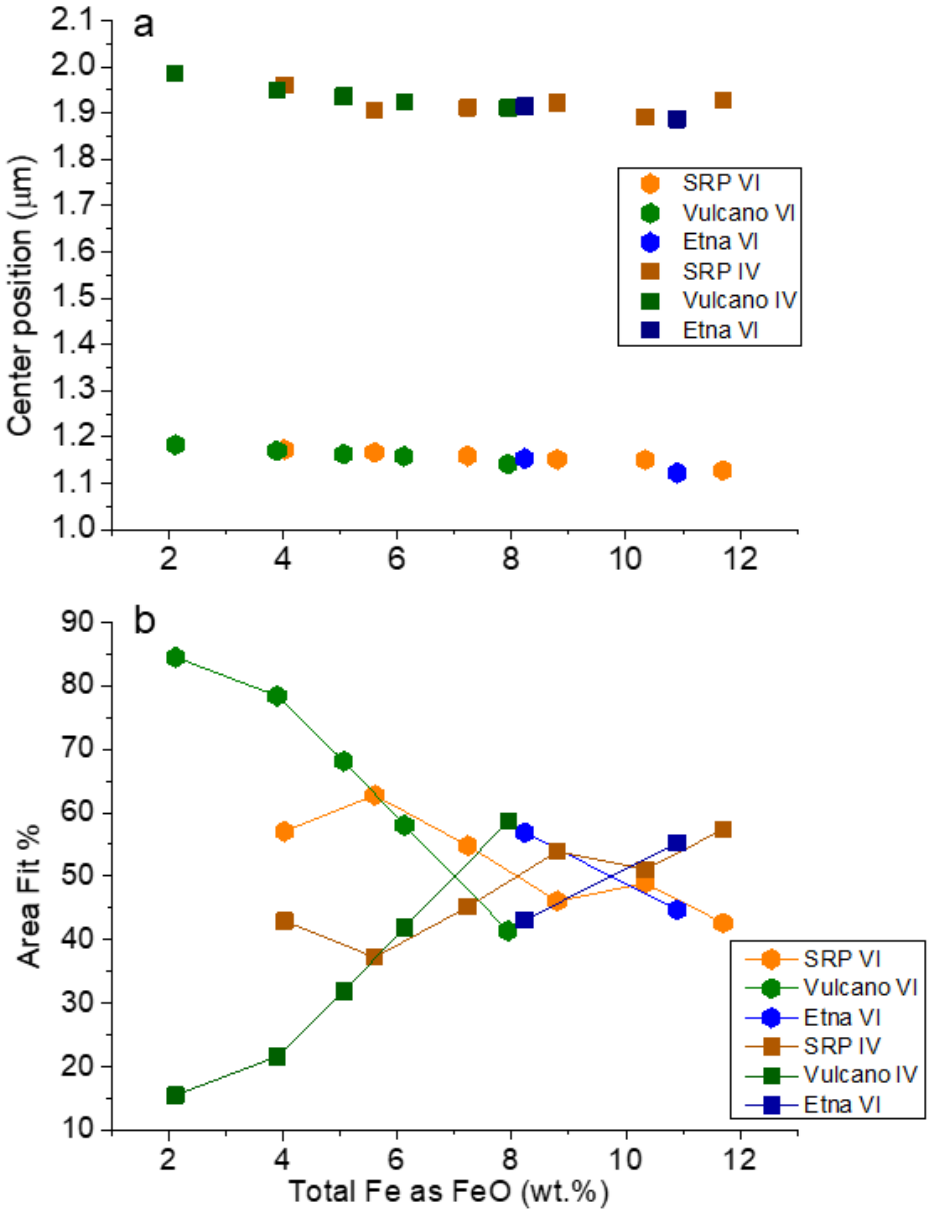

Figure 6: *Variation of centres of absorption (above) and area percentage (below) in relationship with total iron content changing.*

	SiO_2	TO_2	Al_2O_3	FeO^a	MnO	MgO	CaO	Na_2O	K_2O	P_2O_5	$FeIII/Fe_{tot}{}^b$	SCFM
B	48.32	1.82	16.23	11.70	0.18	7.62	10.81	2.57	0.36	0.34	0.61	0.68
	0.15	0.05	0.08	0.10	0.03	0.05	0.07	0.05	0.02	0.03		
B8	53.06	1.60	15.52	10.34	0.15	6.14	8.88	2.69	1.22	0.29	0.63	0.74
	0.11	0.04	0.09	0.08	0.05	0.04	0.07	0.07	0.04	0.03		
B6	57.75	1.35	14.94	8.80	0.13	4.68	7.08	2.83	2.08	0.24	0.70	0.80
	0.16	0.04	0.08	0.11	0.03	0.05	0.08	0.06	0.04	0.03		
B4	62.68	1.11	14.26	7.23	0.10	3.19	5.26	2.91	2.97	0.22	-	-
	0.21	0.04	0.09	0.12	0.02	0.05	0.07	0.07	0.06	0.03		
B2	67.49	0.88	13.71	5.60	0.08	1.70	3.42	3.05	3.84	0.17	-	-
	0.17	0.03	0.06	0.11	0.02	0.03	0.05	0.06	0.07	0.02		
RB	72.13	0.65	13.20	4.02	0.04	0.25	1.62	3.17	4.75	0.14	0.59	0.95
	0.10	0.03	0.06	0.08	0.03	0.01	0.03	0.05	0.05	0.02		
S	54.23	0.69	16.02	7.94	0.17	4.13	7.68	5.34	3.11	0.49	-	-
	0.20	0.03	0.11	0.11	0.04	0.05	0.09	0.14	0.04	0.03		
S7	60.38	0.51	15.37	6.12	0.14	2.94	5.71	4.84	3.63	0.29	0.71	0.85
	0.20	0.02	0.08	0.14	0.02	0.04	0.10	0.09	0.05	0.03		
S5	63.83	0.39	14.78	5.06	0.12	2.17	4.44	4.68	4.08	0.27	0.72	0.89
	0.24	0.02	0.09	0.08	0.03	0.03	0.07	0.27	0.07	0.03		
S3	67.57	0.29	14.28	3.90	0.10	1.40	3.09	4.49	4.51	0.18	0.71	0.92
	0.11	0.02	0.09	0.09	0.03	0.03	0.05	0.06	0.05	0.02		
RS	73.25	0.12	13.53	2.12	0.07	0.25	1.12	4.17	5.13	0.047	0.61	0.97
	0.08	0.02	0.08	0.07	0.02	0.02	0.03	0.06	0.05	0.02		
M	48.50	1.53	14.53	10.90	0.18	7.82	12.13	2.61	1.23	0.45	0.66	0.67
	0.18	0.04	0.08	0.11	0.02	0.07	0.13	0.04	0.03	0.03		
M5	55.36	1.36	15.64	8.23	0.17	4.58	7.62	4.34	2.20	0.37	0.65	0.79
	0.14	0.05	0.12	0.16	0.02	0.05	0.11	0.07	0.02	0.03		
V	63.25	1.20	17.11	5.05	0.17	1.45	3.18	4.92	3.22	0.35	0.61	0.91
	0.25	0.04	0.05	0.08	0.03	0.03	0.05	0.16	0.05	0.04		

Table 1: Chemical composition of investigated products. For oxide, relative abundance in Wt.% is reported together with the standard deviation of the same value over five measurements. [a]refers to total iron taken into account as FeO, [b]reports measured iron speciation. SCFM refers to the parameter defined by Walter and Salisbury (1989): $SiO_2/(SiO_2+CaO+FeO+MgO)$ with oxides accounted as Wt.%. For *B2*, *B4* and *S* it was not possible to calculate Fe_{III}/Fe_{tot}, due to insufficient sample amount, and therefore SCFM is missing as well.

	WL/range	B	B8	B6	B4	B2	R	S	S7	S5	S3	R	M	M5
VIS slope	0.5-0.8 μm	0.35	0.34	0.45	0.41	0.46	0.56	0.52	0.47	0.46	0.40	0.25	0.33	0.44
σ VIS slope		0.0007	0.0005	0.0009	0.0007	0.0008	0.0007	0.0017	0.0013	0.0012	0.0010	0.0007	0.0007	0.000
NIR slope	1.2-1.8 μm	0.21	0.19	0.21	0.19	0.17	0.15	0.17	0.17	0.18	0.16	0.15	0.16	0.18
σ NIR slope		0.0002	0.0001	0.0002	0.0002	0.0001	0.0002	0.0002	0.0002	0.0002	0.0001	0.0001	0.0002	0.000
VNIR slope	0.6-2.0 μm	0.22	0.20	0.23	0.20	0.19	0.20	0.20	0.19	0.18	0.15	0.10	0.18	0.19
σ VNIR slope		0.0001	0.0001	0.0002	0.0001	0.0001	0.0002	0.0001	0.0002	0.0002	0.0002	0.0002	0.0001	0.000
VIS albedo	0.8 μm ref.	0.23	0.22	0.30	0.31	0.40	0.57	0.50	0.52	0.56	0.64	0.70	0.20	0.26
σ Vis albedo		0.0016	0.0016	0.0018	0.0015	0.0018	0.0026	0.0017	0.0015	0.0014	0.0012	0.0006	0.0013	0.001
NIR albedo	1.62 μm ref.	0.44	0.40	0.50	0.48	0.55	0.71	0.67	0.67	0.70	0.75	0.76	0.38	0.42
σ NIR albedo		0.0002	0.0003	0.0002	0.0002	0.0004	0.0002	0.0005	0.0003	0.0002	0.0003	0.0002	0.0002	0.000
$R_{1.55}/R_{0.8}$	Ratio of ref. at 1.55 and 0.8 μm	1.90	1.82	1.65	1.50	1.36	1.23	1.35	1.29	1.25	1.17	1.08	1.85	1.55
		0.0006	0.0007	0.0008	0.0006	0.0007	0.0011	0.0008	0.0009	0.0009	0.0009	0.0007	0.0004	0.000

Table 2: Values of slopes, albedoes, and spectral ratio for each sample, with relative errors σ as defined within De Angelis et al. 2014. For $R_{1.55}/R_{0.8}$, σ is calculated from the albedo errors at 1.55 and 0.8 μm following the rule of error propagation in a ratio.

	B	B8	B6	B4	B2	R	S	S7	S5	S3	RS	M	M5
Octahedral absorption Fe^{2+}													
Area Fit	0.0109	0.0074	0.0073	0.0092	0.0082	0.0075	0.0061	0.0086	0.0106	0.0107	0.0166	0.0068	0.0055
Area Fit%	42.65	48.92	46.08	54.82	62.76	57.06	41.39	58.03	68.13	78.42	84.50	44.72	56.88
Center Max	1.13	1.15	1.15	1.16	1.17	1.17	1.14	1.16	1.16	1.17	1.18	1.12	1.15
Max Height	0.0277	0.0205	0.0212	0.0267	0.0252	0.0237	0.0181	0.0250	0.0298	0.0299	0.0409	0.0198	0.0159
FWHM	0.37	0.34	0.33	0.33	0.31	0.30	0.32	0.32	0.34	0.34	0.39	0.32	0.33
Tetrahedral absorption Fe^{2+}													
Area Fit	0.0147	0.0077	0.0085	0.0076	0.0049	0.0057	0.0087	0.0062	0.0050	0.0030	0.0031	0.0084	0.0042
Area Fit%	57.35	51.08	53.92	45.18	37.24	42.94	58.61	41.97	31.87	21.58	15.50	55.28	43.12
Center Max	1.93	1.89	1.92	1.91	1.91	1.96	1.91	1.92	1.94	1.95	1.99	1.89	1.92
Max Height	0.0305	0.0185	0.0193	0.0184	0.0126	0.0127	0.0186	0.0141	0.0116	0.0073	0.0095	0.0205	0.0100
FWHM	0.45	0.39	0.42	0.39	0.36	0.43	0.45	0.43	0.41	0.38	0.31	0.39	0.39

Table 3: Parameters obtained from fitting processes on the two areas of absorption